Environmental Science & Technology

pubs.acs.org/est

Article

Escalating Carbon Export from High-Elevation Rivers in a Warming Climate

Sen Xu, Si-Liang Li,* Aaron Bufe, Marcus Klaus, Jun Zhong, Hang Wen, Shuai Chen, and Li Li

Cite This: *Environ. Sci. Technol.* 2024, 58, 7032−7044

Read Online

ACCESS | Metrics & More | Article Recommendations | Supporting Information

ABSTRACT: High-elevation mountains have experienced disproportionately rapid warming, yet the effect of warming on the lateral export of terrestrial carbon to rivers remains poorly explored and understood in these regions. Here, we present a long-term data set of dissolved inorganic carbon (DIC) and a more detailed, short-term data set of DIC, $\delta^{13}C_{DIC}$, and organic carbon from two major rivers of the Qinghai−Tibetan Plateau, the Jinsha River (JSR) and the Yalong River (YLR). In the higher-elevation JSR with ∼51% continuous permafrost coverage, warming (>3 °C) and increasing precipitation coincided with substantially increased DIC concentrations by 35% and fluxes by 110%. In the lower-elevation YLR with ∼14% continuous permafrost, such increases did not occur despite a comparable extent of warming. Riverine concentrations of dissolved and particulate organic carbon increased with discharge (mobilization) in both rivers. In the JSR, DIC concentrations transitioned from dilution (decreasing concentration with discharge) in earlier, colder years to chemostasis (relatively constant concentration) in later, warmer years. This changing pattern, together with lighter $\delta^{13}C_{DIC}$ under high discharge, suggests that permafrost thawing boosts DIC production and export via enhancing soil respiration and weathering. These findings reveal the predominant role of warming in altering carbon lateral export by escalating concentrations and fluxes and modifying export patterns.

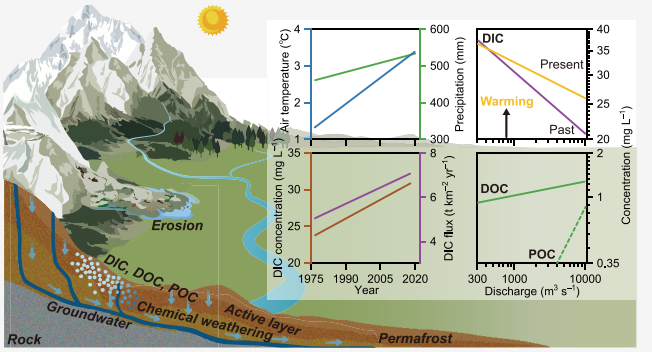

KEYWORDS: *carbon cycle, carbon isotope, concentration−discharge relationship, climate change, Qinghai−Tibet Plateau*

1. INTRODUCTION

Riverine carbon species, including dissolved inorganic and organic carbon (DIC and DOC) and particulate organic carbon (POC), constitute crucial components of the global carbon cycle connecting the land to the ocean.[1−6] Globally, exorheic rivers export about 0.38 Pg C yr^{-1} of DIC to the coastal ocean, mainly in the form of hydrogen carbonate (HCO_3^-).[1] Riverine DIC can originate from rock weathering (geogenic) or from soil respiration (biogenic)[4,6,7] and can act as a tracer of climate change impacts on the critical zone and fluvial biogeochemistry.[8−10] Riverine DOC and POC are reactive portions of laterally transferred carbon, playing a significant role in the carbon cycle of inland waters and coastal environments.[1−5] The production and export of riverine carbon depend on temperature and water flow, often driven by seasonal weather, long-term climate changes, and associated earth surface processes such as permafrost thaw,[8,11−16] reflecting the earth's surface responses to climate change and human perturbations.[2,6,8−10,17−20] For example, DOC can be rapidly mineralized or transported over long distances after being produced or released from soil organic carbon (SOC) during permafrost degradation.[13,21] The substantial amount of SOC in permafrost regions therefore represents an important potential carbon source in a warming climate.[14,21,22] Understanding the interactive drivers and processes of carbon production and export is critical to constraining the role of anthropogenic climate change on riverine carbon fluxes.

The Arctic region has shown clear decadal increases in DIC and alkalinity fluxes across major rivers including the Mackenzie, Yenisei, and Ob Rivers in a warming climate.[8−10] Outside the Arctic, high-elevation and mountainous regions experience the most rapid climate warming.[23−25] Such regions potentially act as sentinel sites, offering early glimpses of climate change impacts on fluvial biogeochemistry.[18,26] The Qinghai−Tibetan Plateau (QTP), referred to as the "Earth's Third Pole" and "Asian Water Tower", stands as the highest and most extensive orogenic plateau in the world.[23,27] Over the past four decades, warming has elevated air temperature and moisture in the QTP, affecting local atmospheric, hydrological, and biogeochemical cycles.[22,23,28,29] Observed consequences include glacial shrinkage,[23,30] permafrost degradation,[31] lake

Received: August 18, 2023
Revised: March 25, 2024
Accepted: March 29, 2024
Published: April 11, 2024

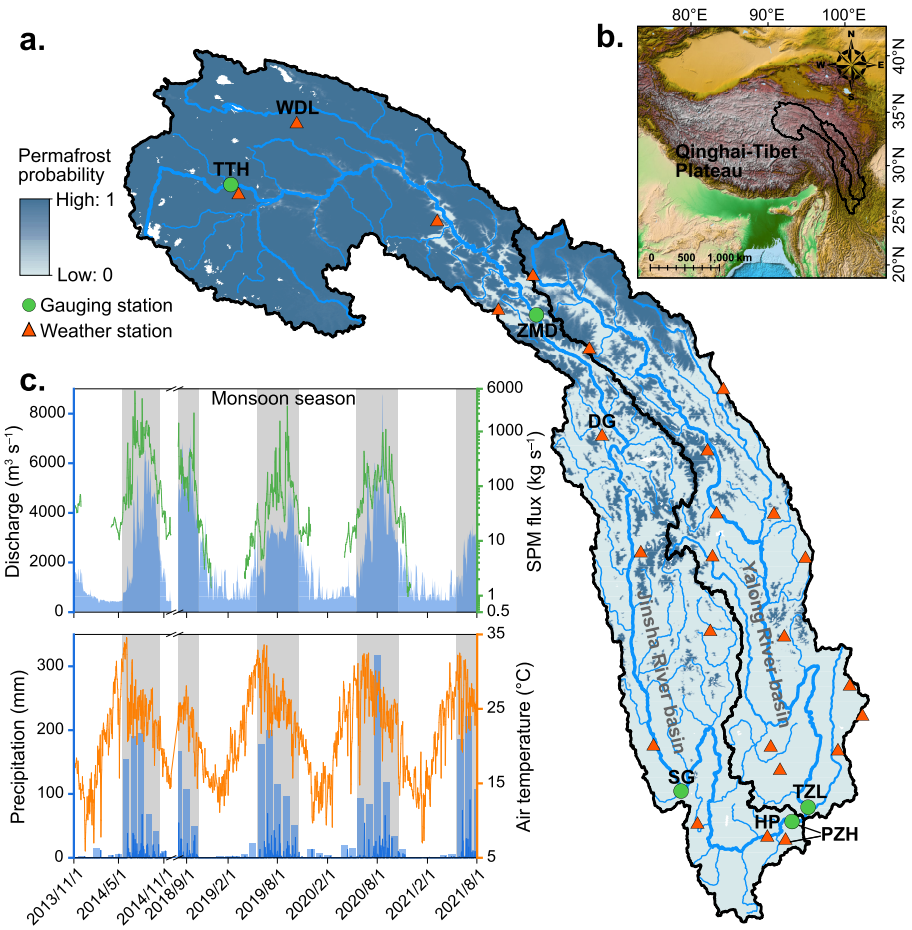

Figure 1. Study region, station locations, and climate records. (a) Map showing the distribution of permafrost extent and the locations of weather and gauging stations. The analysis was focused on the meteorological data from Wudaoliang (WDL), Tuotuohe (TTH), Dege (DG), Huaping (HP), and Panzhihua (PZH) weather stations and the hydrological data from TTH, Zhimenda (ZMD), Shigu (SG), PZH, and Tongzilin (TZL) gauging stations. The permafrost probability (fraction values from 0 to 1) is defined as continuous permafrost (>0.9), discontinuous permafrost (0.5−0.9), sporadic permafrost (0.1−0.5), and isolated patches (0.005−0.1).[43] The map's gradient from dark to light blue illustrates the transition from permafrost-dominated conditions to isolated permafrost. (b) Regional overview of the Jinsha and Yalong River basins within the Qinghai−Tibet Plateau. (c) Temporal variations in daily mean discharge, suspended particulate matter (SPM) flux, daily mean air temperature, and daily and monthly (blue column) precipitation measured at the PZH gauging and weather stations. The monsoon seasons (from June to October) are shaded in gray.

growth,[24,32] thermokarst lake formation,[33] and increased runoff and sediment fluxes.[23,25,34,35] Furthermore, warming has enhanced net primary production and soil respiration and changed greenhouse gas emissions (CO_2, CH_4, and N_2O) from the land to the atmosphere.[13,29,36] These environmental changes could enhance chemical weathering, modulate solute production and transport, and intensify biogeochemical carbon cycles because warming increases soil respiration and mineral dissolution kinetics, and permafrost degradation exposes unweathered minerals.[10,12,37]

Despite a comprehensive knowledge of hydrologic responses to warming,[23,25,27,34,35] the responses of fluvial biogeochemistry to warming remain poorly constrained in the QTP and in other high-elevation landscapes outside the Arctic. Consistent long-term observations of fluvial carbon fluxes from these regions are rare, thereby limiting our understanding of the impact of climate change on fluvial carbon export and its future trends.[18,26] To interpret long-term changes in carbon fluxes in the context of climate change, observations on the short-term climatic sensitivity of fluvial carbon export are needed, and such observations are particularly limited in these regions.[11,38] This lack of observations is partly due to the scarcity of long-term and continuous biogeochemical measurements in high-elevation rivers that are usually located in remote regions. Data collection in such regions poses significant challenges and requires substantial logistical efforts. In the QTP, existing studies have primarily focused on the relationship between fluvial dissolved carbon export and seasonal variability in weather conditions,[11,15,38−42] and primarily based on a limited total number of samples[41,42] or on a limited number of sampled years.[11,15,38−40] Limited time-series data introduce considerable uncertainties in flux calculations and biogeochemical process analyses, preventing an analysis of the long-term impact of climate warming on fluvial biogeochemistry. In addition, existing studies have reported the seasonal export of either DIC or DOC; the total export of riverine carbon, including both dissolved and particulate forms, has not yet been quantified.

To address these limitations, we analyze both a decade-long time series of fluvial DIC export and seasonal covariation of fluvial DIC, DOC, and POC exports from two large rivers draining the QTP: the Jinsha River (JSR) and the Yalong River

https://doi.org/10.1021/acs.est.3c06777
Environ. Sci. Technol. 2024, 58, 7032−7044

(YLR). The decade-long data on DIC fluxes span four decades for the JSR (1977−2018) and cover a shorter historical period for the YLR (1973−1985). The seasonal data set covers four years (2013−2014 and 2018−2021) for both rivers. These two data sets allow us to evaluate the variations, trends, and drivers of carbon export on both multidecadal and seasonal time scales and to understand the dynamics of fluvial carbon export responding to climate change.

2. METHODS

2.1. Study Area. Riverine carbon dynamics were measured in two large rivers, the JSR and YLR, situated in the upper Yangtze River Basin (Figure 1a,b). The JSR is the upper stretch of the Yangtze River, originating from the Jianggudiru Glacier on Mt. Geladandong. It drains an area of 259,177 km^2 above the Panzhihua (PZH) gauging station with an average elevation of 4267 m. The YLR is the largest tributary of the JSR, originating from Mt. Bayan Kara and draining an area of 128,363 km^2 above the Tongzilin (TZL) gauging station with an average elevation of 3799 m. Our sampling sites are located upstream of the confluence of these two rivers near Panzhihua City (Figure 1a).

About half of the JSR basin is underlain by continuous permafrost (∼51%; Figure 1a, where a permafrost probability exceeding 0.9 is defined as continuous permafrost), whereas only ∼14% of the YLR basin area is covered by continuous permafrost. The JSR can be divided into three sections based on topography and climate: the headwater region (above the Zhimenda (ZMD) gauging station), the middle region (from ZMD to Shigu (SG) gauging station), and the lower region (from SG to PZH) (Figure 1a). The headwater region lies in an arid zone and features extensive glaciers, continuous permafrost, evaporite deposits, and saline lakes.[24,43,44] In contrast, the middle and lower regions lie in a wet climate zone dominated by the Indian monsoon[28] and predominantly underlain by metamorphic (e.g., sandstones) and carbonate rocks.[45] The majority of the annual discharge of the JSR occurs during the monsoon season from June to October (e.g., 66% in 2019) (Figure 1c). The YLR drains plateau regions at elevations lower than the JSR and experiences a cold and dry climate in the upper reaches and a warm and wet climate in the lower reaches.[38] Due to different extents and distributions of glaciers, snow, and permafrost in the headwater regions, seasonal discharge changes between these two rivers differ. Runoff in the YLR basin is approximately twice that in the JSR basin (Table S1), and the former represents a more humid environment than the latter.

2.2. Data Acquisition. A data set of long-term measurements (LTMs; Table S1) for major ion chemistry at the JSR outlet (PZH gauging station, formerly Dukou station until 1987) during the period 1977−2018 and the YLR outlet (Xiaodeshi gauging station, near TZL gauging station) during the period 1973−1985 was retrieved from Hydrological Yearbooks (details of the data set are provided in Supporting Text S1). These yearbooks were produced annually by the Changjiang Water Resources Commission for internal use. Water temperature, pH, electrical conductivity, and discharge measured at each sampling event were also extracted from these yearbooks. The sampling frequency was mainly once a month, with 12 samples per year from 1987 to 2018, resulting in 506 measurements for the JSR and 154 measurements for the YLR. The sampling and analysis procedures have been detailed previously.[46] Chemical analyses of water samples were performed following standard procedures and protocols.[47] The reliability of these historical records has been assured through previous comparisons of the results measured at the same time and location but by different agencies.[46,47] Additionally, the major element concentrations and electrical conductivity in the JSR from the yearbooks during the periods from November 2013 to October 2014 and August to December 2018 align well with the measurements from this study (Figure S1), further supporting the quality of the yearbook reports. The sources of hydrometeorological data used in this study are provided in Supporting Text S2.

2.3. Fieldwork and Laboratory Analyses. In addition to compiling the long-term data set, we collected surface river water samples from the JSR and YLR above their confluence at Panzhihua City (Figure 1a; 30 and 20 km from Panzhihua City and near PZH and TZL gauging stations, respectively). River waters were sampled and analyzed from November 2013 to October 2014 and August 2018 to June 2021 (defined as short-term measurements (STMs) relative to the LTMs in this study; Table S2). Sampling frequency was generally once a month but increased to once a week or more frequently during the monsoon season due to high hydrologic variability. Water temperature and pH were measured in the field using a WTW3210 pH meter. Samples were filtered through 0.45 μm nitrocellulose filters and 0.7 μm precombusted glass fiber filters, split into multiple aliquots for different measurements, and stored in clean, air-free bottles.

Alkalinity was measured by titration with 0.02 mol L^{-1} HCl in the field within 24 h after sampling with three replicates, and DIC concentration was calculated from pH, water temperature, and alkalinity using the CO2SYS program.[48] Titration is a common method for alkalinity measurement in long-term data sets, and calculated DIC concentration can provide valuable insights in the absence of direct measurements.[6,49] DOC concentrations were measured on an Aurora 1030 total OC analyzer (OI Analytical) with duplicates (±1.5%, analytical error). Concentrations of suspended particulate matter (SPM) were measured by freeze-drying and weighing the glass fiber filters. The SPM retained on the filter was scraped, treated with HCl to remove inorganic carbon, and used to measure the content of POC (POC%) using an elemental analyzer (Vario EL III, Elementar) (±5%, analytical error). To analyze the $\delta^{13}C$ of DIC ($\delta^{13}C_{DIC}$), water samples were injected with a syringe into glass bottles that were prefilled with phosphoric acid and magnetic stir bars.[38] The CO_2 was then extracted and purified in a vacuum system and transferred into a tube for $\delta^{13}C_{DIC}$ measurement using a Finnigan MAT 252 mass spectrometer. The result was reported using the δ notation relative to the Vienna Pee Dee Belemnite (V-PDB) with an accuracy of 0.1‰.

2.4. Data Analyses. The LTM data set comprises alkalinity concentrations in the JSR from 1977 to 2005. To infer alkalinity concentrations from 2006 onward for the LTM data set, we employed a multiple linear stepwise regression (MLR) model for the river chemistry data (refer to Supporting Text S1). The selected final models were utilized to infer alkalinity concentrations (the selected models are listed in Table S3).

We analyzed linear trends of variables over time using the Theil Sen estimator (Table S4). We evaluated the statistical significance (p) of the linear trends using a modified two-tailed Mann−Kendall (MK) test, which accommodates missing

https://doi.org/10.1021/acs.est.3c06777
Environ. Sci. Technol. 2024, 58, 7032−7044

values and accounts for serial correlation through a variance correction approach (refer to Supporting Text S3).[50]

We estimated the relative contribution of changes in temperature and precipitation to the observed change in DIC flux in the JSR by analyzing the cumulative anomalies and the slope change ratios of the cumulative quantities between 1977−1997 and 1998−2018 (refer to Supporting Text S4).[51] Analogously, we also estimated the relative contribution of changes in DIC concentrations and runoff to the DIC flux change.

We calculated the basin-averaged air temperature and precipitation in the JSR and YLR basins using the Thiessen polygon method in ArcGIS version 10.2 based on meteorological data from 13 and 12 weather stations, respectively (Figure 1a and Table S1). The annual meteorological data underwent preprocessing with quality control, excluding annual data that deviated considerably from historical records due to incomplete daily scale data in that year.

Concentration (or isotopic value)−discharge ($C-Q$ *or* $I-Q$) relationships and the ratio of coefficients of variation in concentration and discharge (CV_C/CV_Q) were employed to quantify carbon export regimes,[52,53] reflecting the responses of instantaneous concentrations to hydrologic changes. The power law slope (b) refers to the slope of the log-transformed $C-Q$ relationship and, together with CV_C/CV_Q, was used to determine export regimes of solutes, including dilution, chemostasis, and mobilization (refer to Supporting Text S5).[52]

2.5. Estimation of DIC, DOC, and POC Fluxes. For the STM data during the periods 2013−2014 and 2018−2021, we utilized the U.S. Geological Survey (USGS) Load Estimator (LOADEST) program to estimate DIC, DOC, and POC fluxes of rivers based on the measured concentrations. LOADEST uses continuous daily discharge and discrete DIC, DOC, and POC concentration data to derive flux estimates by automatically selecting the best regression model from nine options based on the Akaike information criterion (AIC). The LOADEST-modeled daily loads can be used to estimate fluxes at the monthly, seasonal, and annual time scales. The LOADEST models selected for flux calculation are listed in Table S5.

For the LTM data, due to the unavailability of continuous daily discharge data and consistent sampling time and frequency across different years, we combined the annual discharge-weighted mean concentration (C_{dwm}) of DIC and runoff to estimate the annual flux of DIC (Table S1). The C_{dwm} of DIC was calculated as follows:

$$C_{dwm} = \frac{\sum_{i=1}^{n} C_i \times q_i}{\sum_{i=1}^{n} q_i} \quad (1)$$

We also calculated the annual arithmetic mean concentration (C_{am}) of DIC as follows:

$$C_{am} = \frac{\sum_{i=1}^{n} C_i}{n} \quad (2)$$

where C_i and q_i are the DIC concentration of sample i and the instantaneous discharge, respectively, and n is the sample size for each year. For the calculations of C_{am} and C_{dwm} of DIC in 2013−2014, 2019, and 2020 for the STM data set, we selected data near the middle of each month instead of using all the data to maintain consistency with the time and frequency of the LTM data.

The DIC flux (F) of the year i was then calculated as follows:

$$F = C_{dwm} \times Q_i \quad (3)$$

where Q_i is the total runoff of the year i. We calculated the DIC flux at average runoff (F_{avgR}) of the year i as follows:

$$F_{avgR} = C_{dwm} \times Q_m \quad (4)$$

where Q_m is the average runoff during the LTM data covered period (Table S1).

3. RESULTS

3.1. Rapid Warming and Hydrologic Changes in the Upper Yangtze River Basin. The high-elevation QTP has experienced significant warming.[23,32] Since the 1950s, the average air temperature has risen by 1.9 °C, with a warming rate of 0.032 °C yr^{-1}, which is twice the global average warming rate.[54] Notably, since the 1980s, the warming rate in this region has been unparalleled in the last two millennia,[25] reaching 0.044 °C yr^{-1} during 1980−2018, as recorded by 95 China Meteorological Administration weather stations.[32]

The basin-averaged air temperature in the JSR basin displayed a considerable warming trend during 1977−2020 (MK: p = 0.000), with an increase of 3.02 °C and a warming rate of 0.048 °C yr^{-1}, surpassing the aforementioned warming rates (Figure 2a). In the YLR basin, basin-averaged air temperature increased by 2.13 °C, with a warming rate of 0.036 °C yr^{-1} during 1973−2020 (Figure S2a). The warming rates differ in different regions (Figures 1a and S3). In the headwater region of the JSR, the annual mean air temperature increased rapidly, with rates of 0.047 and 0.042 °C yr^{-1} recorded at the Tuotuohe (TTH) and Wudaoliang (WDL) weather stations, respectively. Furthermore, the annual mean ground temperature also increased rapidly at the upstream stations (0.057 °C yr^{-1} at the TTH and 0.059 °C yr^{-1} at the WDL) (Figures 1a and S3). In contrast, the air temperature increased relatively slowly in the middle and lower regions of the JSR basin (0.03 °C yr^{-1} at the Dege (DG) and 0.014 °C yr^{-1} at the Huaping (HP)).

In addition to warming, the QTP has experienced overall increasing precipitation.[28,55] In the JSR basin, the basin-averaged precipitation increased by 1.7 mm yr^{-1} during 1977−2020 (MK: p = 0.002) (Figure 2b). For the YLR basin during 1973−2020, the increasing rate was 1.1 mm yr^{-1} (Figure S2b). This rate of increase was even higher in the headwaters with 3.8 mm yr^{-1} (WDL) and 2.6 mm yr^{-1} (TTH) at the upstream stations, compared to a lower rate of 1.9 mm yr^{-1} at the midstream station (DG), and a lack of observable increase at the downstream station (HP) (Figure S3). These spatial differences in temperature and precipitation changes indicate a pronounced and profound warming and wetting trend in the high-elevation headwater regions of the JSR and YLR basins.

In response to rapid warming and wetting, the cryosphere in the QTP has rapidly shrunk over the last decades through glacier recession, snowmelt, and permafrost thaw.[23,25,30,31] These changes have substantially elevated fluvial water and sediment fluxes.[23,25,34,35] Our analyses revealed an average increasing rate of 3.0×10^7 m^3 yr^{-1} in annual discharge and 3.8×10^4 t yr^{-1} in annual sediment load in the JSR headwater region (upstream gauging station, TTH) (Figure S4). In the middle and lower regions of the JSR basin (ZMD and SG gauging stations), annual discharge and sediment load still

https://doi.org/10.1021/acs.est.3c06777
Environ. Sci. Technol. 2024, 58, 7032−7044

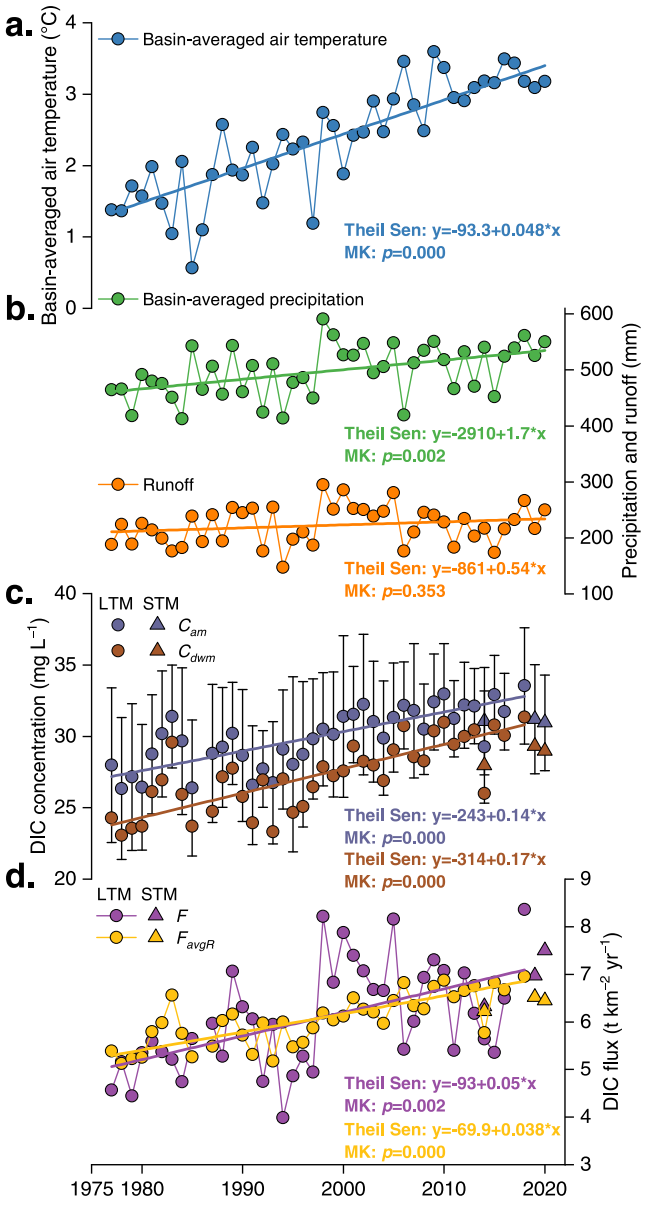

Figure 2. Long-term trends of variables in the Jinsha River Basin. (a) Basin-averaged air temperature. (b) Basin-averaged precipitation and runoff. (c) Annual arithmetic mean (C_{am}) and discharge-weighted mean (C_{dwm}) concentrations of DIC. (d) DIC flux (F) and the DIC flux calculated at average runoff (F_{avgR}). The basin-averaged air temperature and precipitation were calculated by the Thiessen polygon method based on meteorological data from 13 weather stations (Figure 1a) from 1977 to 2020. Runoff (annual discharge normalized by drainage area) was measured at the Panzhihua (PZH) gauging station. Long-term measurements (LTMs) and short-term measurements (STMs) of the DIC concentration and flux were plotted together, but linear trends were analyzed for the LTM data only. Black error bars represent standard deviations of the C_{am}. We calculated Theil Sen trend lines for the variables and evaluated the statistical significance (p) of the linear trends using a modified two-tailed Mann−Kendall (MK) test.

showed an increasing trend, but the rates were lower than those at the upstream station. Consequently, a potential slight increase of runoff from the JSR basin by 0.54 mm yr^{-1} from 1977 to 2020 remained uncertain (MK: p = 0.353) (Figure 2b). The sediment load recorded at the PZH station however experienced a sharp decrease after 2009 due to damming (Figure S4).

3.2. Long-Term Trends of DIC Concentration and Flux. Understanding the impact of warming on fluvial carbon export requires long-term observations. The LTM data set reveals a significant increase in the concentration and flux of DIC in the JSR from 1977 to 2021 (Figure 2c,d; monthly LTM data shown in Figure 3a; monthly STM data shown in Figure 4a). Over the entire observation period, the C_{am} of DIC increased by 27%, from 26.3 to 33.5 mg L^{-1}, at an average rate of 0.14 mg L^{-1} yr^{-1} (MK: p = 0.000) (Figure 2c), with particularly substantial increases in the monsoon season when discharge is high (Figure 3b; comparisons of monthly concentrations between periods 1977−1997 and 1998−2018; monthly data for different periods are provided in Table S6). The C_{dwm} of DIC increased by 35%, at a higher rate of 0.17 mg L^{-1} yr^{-1} (MK: p = 0.000) (Figure 2c), highlighting the additive role of discharge. The combination of strongly increasing DIC concentration and slightly increasing runoff led to an increase of the DIC flux (F) of the JSR by 110%, from 4 to 8.4 t km^{-2} yr^{-1}, at an increasing rate of 0.05 t km^{-2} yr^{-1} (MK: p = 0.002) (Figure 2d). The largest fluxes occurred in the years with the highest precipitation and runoff, such as in 1998. The observed increase in DIC flux here is lower than that reported for the Ob (+134%) and Yenisei (+185%) Rivers[8] and higher than that reported for the Mackenzie River (+12.5%).[9]

Due to the limited availability of long-term continuous observation data for the YLR, we were unable to draw definitive conclusions regarding the trends of DIC concentrations and fluxes. However, compared to the corresponding historical records, the STM data showed stable or even slightly decreasing DIC concentrations and constant DIC fluxes (Figures 3c and S2c,d). Additionally, the monthly DIC concentrations of the STM data were mostly lower than those of the historical records except for the months of June and July (Figure 3d), again being consistent with long-term stability or even a decrease of DIC concentrations in the YLR.

3.3. Short-Term Dynamics of DIC, DOC, and POC Concentrations. High-frequency observations for rivers can offer detailed information about the dynamics and drivers of carbon export (Figure 4). In the JSR, DIC concentrations of the STM data varied from 23.3 to 35.7 mg L^{-1} (29.5 ± 3.7 mg L^{-1}), with prominent seasonality and low values in the monsoon season (Figure 4a). In the YLR, DIC concentrations were slightly lower, varying from 19.9 to 32.3 mg L^{-1} (24.6 ± 2.9 mg L^{-1}), and had a similar seasonality to that of the JSR (Figure 4b). The seasonal variation in DIC concentrations was gradual, typically increasing from the middle of the monsoon season until the end of the dry season. $\delta^{13}C_{DIC}$ is commonly used to trace riverine DIC origins and biogeochemical processes. In the JSR, $\delta^{13}C_{DIC}$ values varied from −7.4 to −2.2‰ (−4.1 ± 1.1‰), with lighter values in the monsoon season (Figure 4a). The YLR had overall lighter $\delta^{13}C_{DIC}$ values than the JSR, ranging from −9.8 to −4.5‰ (−6.4 ± 1.1‰), but both rivers exhibited a similar seasonal variation in $\delta^{13}C_{DIC}$ (Figure 4b). The temporal variation in $\delta^{13}C_{DIC}$ was found to be gradual and highly synchronized with the variation in DIC concentrations (Figure 4).

DOC concentrations ranged from 0.5 to 2.7 mg L^{-1} (1.1 ± 0.4 mg L^{-1}) in the JSR and from 0.6 to 3.9 mg L^{-1} with the same mean concentration (1.1 ± 0.4 mg L^{-1}) in the YLR. The DOC concentrations typically increased from the middle of the dry season until the middle of the monsoon season (Figure 4),

https://doi.org/10.1021/acs.est.3c06777
Environ. Sci. Technol. 2024, 58, 7032−7044

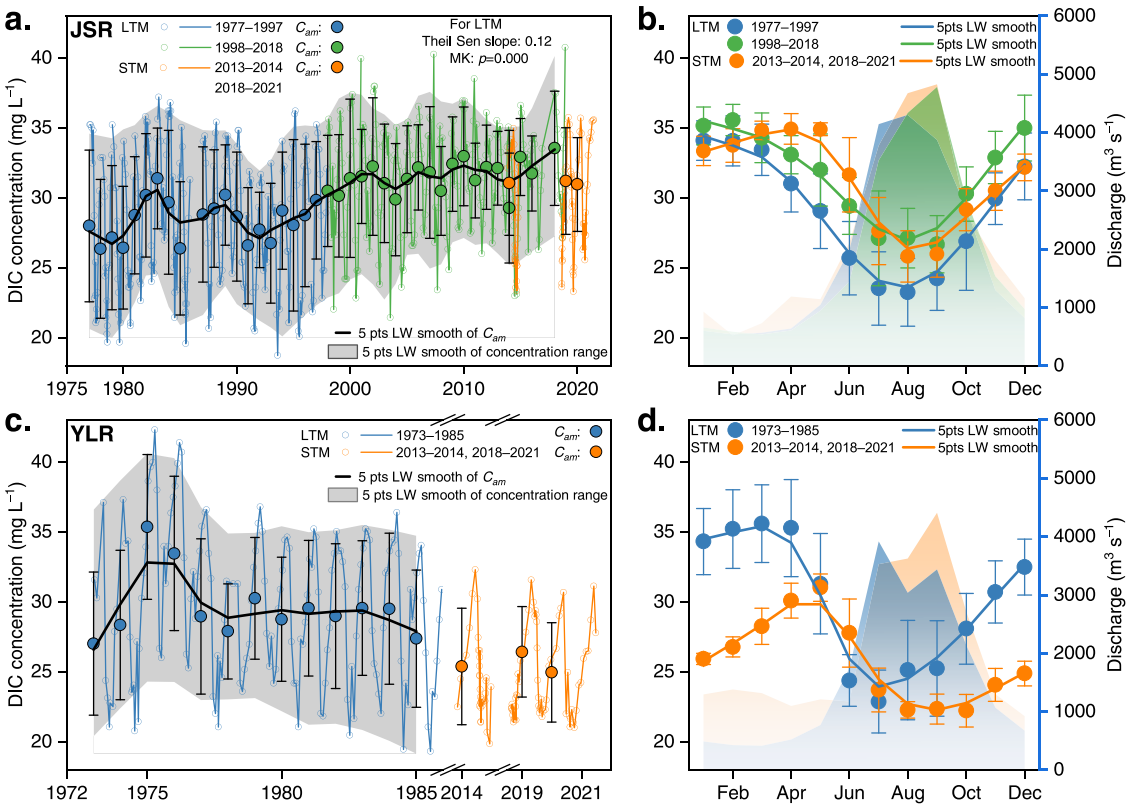

Figure 3. Long-term trends of DIC concentrations in the (a, b) Jinsha River (JSR) and (c, d) Yalong River (YLR). (a, c) Time-series concentrations of DIC (monthly and annual arithmetic mean (C_{am})). (b, d) Multiyear mean monthly concentrations of DIC. Long-term measurements (LTMs) and short-term measurements (STMs) of the DIC concentration were plotted together. Multiyear mean monthly discharge data (shaded areas) were plotted in panels (b) and (d) with the right axis. Five pts LW smoothing (locally weighted scatterplot smoothing, LOWESS) was performed for the LTM of the C_{am} and concentration ranges of DIC and the multiyear mean monthly concentrations of DIC. Black error bars represent standard deviations. We calculated a Theil Sen trend line for the LTM of monthly DIC concentrations in the JSR and evaluated the statistical significance (p) of the linear trend using a modified two-tailed Mann–Kendall (MK) test.

with occasional spikes in the dry season and consistently high concentrations in the monsoon season, contrary to the seasonal variation in DIC concentrations. POC concentrations exhibited a wide range of 0.03–3.4 mg L^{-1} in the JSR and 0.07–3.7 mg L^{-1} in the YLR. The temporal variation in POC concentrations was relatively large, with occasional spikes (Figure 4). Both the concentration and flux of POC peaked in the monsoon season. Carbon fluxes of the JSR were smaller than the YLR, and in the case of 2019, annual DIC, DOC, and POC fluxes, respectively, were 67, 55, and 31% of those of the YLR (Table S1).

4. DISCUSSION

4.1. Hydrologic Regulations of Short-Term Carbon Dynamics. The short-term, seasonal dynamics of dissolved carbon are highly sensitive to hydrologic variability.[11,38,56,57] Riverine DIC originates from biogeochemical processes including rock weathering, soil respiration, water–atmosphere exchange, and in-stream respiration.[4,6,7,58] These different sources and biogeochemical processes can be traced by carbon isotopic compositions because different carbon reservoirs exhibit distinct $\delta^{13}C$ values. For example, carbonate bedrock has a $\delta^{13}C$ value ranging from ∼−2.5 to 0‰.[59] Atmospheric CO_2 exhibits $\delta^{13}C$ values in a narrow range of −8 to −6.5‰.[59] Soil CO_2 has negative $\delta^{13}C$ values ranging from −34 to −24‰, primarily generated through root respiration and heterotrophic respiration of soil organic matter.[60,61] The enrichment of ^{13}C in riverine DIC primarily originates from processes including carbonate weathering,[59] aquatic photosynthesis,[61,62] CO_2 degassing,[63] and metamorphic CO_2 influx.[64]

During the monsoon season, the observed depletion of $\delta^{13}C_{DIC}$ values in the JSR and YLR signifies either a change in the sources of riverine DIC because each source imparts a unique isotopic signal or the occurrence of processes that fractionate carbon isotopes. The main drivers behind these changes may be water (discharge, soil water, and groundwater) and temperature (soil and water temperature) changes and CO_2 exchanges.[11,38,63] The C–Q relationships illustrate how and how much carbon concentrations vary with hydrologic changes (Figure 5). The DIC concentrations and $\delta^{13}C_{DIC}$ values in the JSR and YLR decreased with increasing discharge (Figure 5a–d). The high DIC concentrations and heavy $\delta^{13}C_{DIC}$ values under low discharge likely reflect source waters mostly from groundwater, whereas the low concentrations and light isotopic values under high discharge reflect soil water composition.[7,65]

The DIC concentration and $\delta^{13}C_{DIC}$ show strong chemostatic responses (−0.2 < power law slope (b) < 0.2) with respect to increasing discharge (Figure 5a–d). Multiple processes or a combination of them could cause this chemostatic behavior. Reactive surface areas of minerals and the availability of acidic fluids could be increased during monsoon runoff, thereby releasing the supply and transport limitations of chemical weathering rates.[57,58,66] In particular,

https://doi.org/10.1021/acs.est.3c06777
Environ. Sci. Technol. 2024, 58, 7032–7044

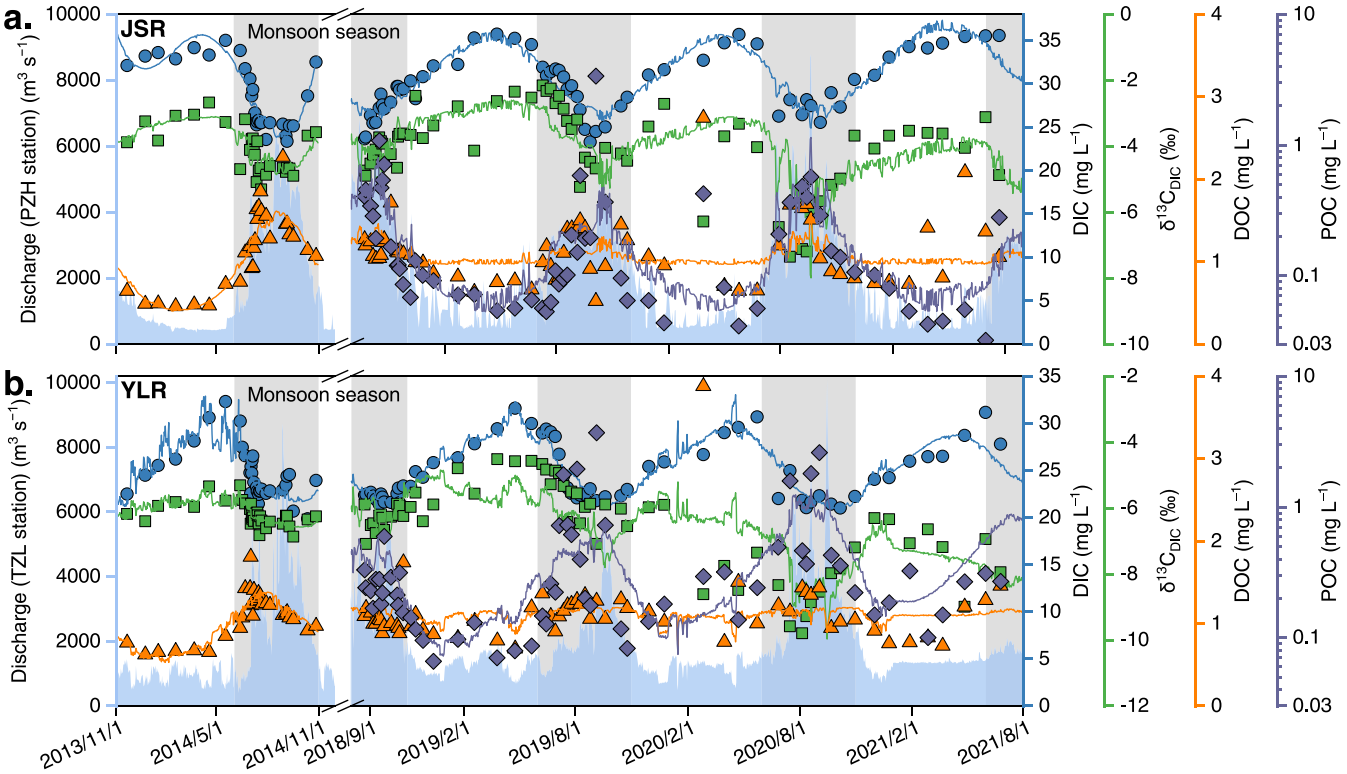

Figure 4. Short-term dynamics of DIC, $\delta^{13}C_{DIC}$, DOC, and POC in the (a) Jinsha River (JSR) and (b) Yalong River (YLR). Short-term measurements (symbols) and LOADEST-modeled daily concentrations (lines) were plotted together. Daily mean discharge data (blue shaded areas) during the sampling periods, measured at the (a) Panzhihua (PZH) and (b) Tongzilin (TZL) gauging stations, were plotted on the left axis. The monsoon seasons (from June to October) are shaded in gray.

the intensity of carbonate weathering could be increased during the monsoon due to higher flow and faster dissolution of carbonate rocks[57] that are distributed widely in the lower regions of the JSR and YLR basins.[38] Moreover, it is possible that DIC concentrations remain relatively constant through the monsoon because the increased runoff suppresses secondary carbonate precipitation in rivers or soils upstream of the sampling sites.[38,63] Finally, the chemostatic behavior could arise from the mobilization of groundwater that carries isotopically positive DIC.[63,65,67,68]

During hydrologic events, the majority of riverine DOC and POC is derived from allochthonous terrestrial carbon, attributable to the elevated transport of SOC.[69−71] In summer, increasing runoff along with rising temperatures stimulates the production of DOC and POC through terrestrial and aquatic photosynthesis.[62,69] Stormflow during the monsoon could transport soil organic matter into rivers via lateral flow through surface soil horizons,[62,69] which may be an important cause for the mobilization pattern of $C-Q$ relationships for DOC and POC observed here (Figure 5e−g). The positive correlations between DOC and discharge identified in this study align with previous findings in the headwater region of the JSR.[39]

During the dry season, when frozen conditions prevail (from November to March, the river channels above ZMD are frozen; Figure 1a), river waters originate dominantly from the middle and lower regions of the JSR and YLR basins. At this time, the contribution of precipitation and meltwater to river water is small, and deep groundwater is a primary contributor to baseflow.[7,58,69] This period manifests simultaneous occurrences of higher DIC concentrations, heavier $\delta^{13}C_{DIC}$ values, and lower DOC and POC concentrations. These variations are consistent with an increased groundwater contribution with DIC inputs from ^{13}C-enriched inorganic sources of carbon, such as carbonate rocks.[7,56,58] The reduced biomass productivity and biological activity in cold winters lead to lower DOC and POC concentrations.[38,70,72] The covariation of carbon concentrations and discharge suggests that hydrologic changes largely regulate the intra-annual dynamics of DIC, DOC, and POC exports.

In addition to hydrologic variability, damming and permafrost thawing in the JSR and YLR basins may influence the seasonal dynamics of the DOC and POC concentrations. A prior study has found older radiocarbon ages of DOC in Tibetan rivers than those in Arctic and tropical rivers and identified a positive relationship between radiocarbon age and permafrost watershed coverage.[42] This correlation is evidence of the export of old carbon from permafrost regions during thawing seasons. In the central QTP permafrost region, the riverine DIC and DOC fluxes increased with thawed depth and decreased with the thickness of the frozen layer, suggesting the importance of changing permafrost for riverine carbon export.[11,15] A large area of continuous permafrost in the JSR source region suggests that the permafrost carbon pool could release DOC and POC to rivers during the thawing periods,[73] with the potential rapid utilization of organic carbon by microbes in permafrost headwaters.[13,21] Additionally, the presence of cascade dams along the JSR (in the section between SG and PZH) and YLR may have influenced the temporal variations of DOC and POC exports.[74] This influence could be particularly notable during the dry season, when reservoirs largely regulate river discharge, leading to larger flows compared to the period prior to dam construction

https://doi.org/10.1021/acs.est.3c06777
Environ. Sci. Technol. 2024, 58, 7032−7044

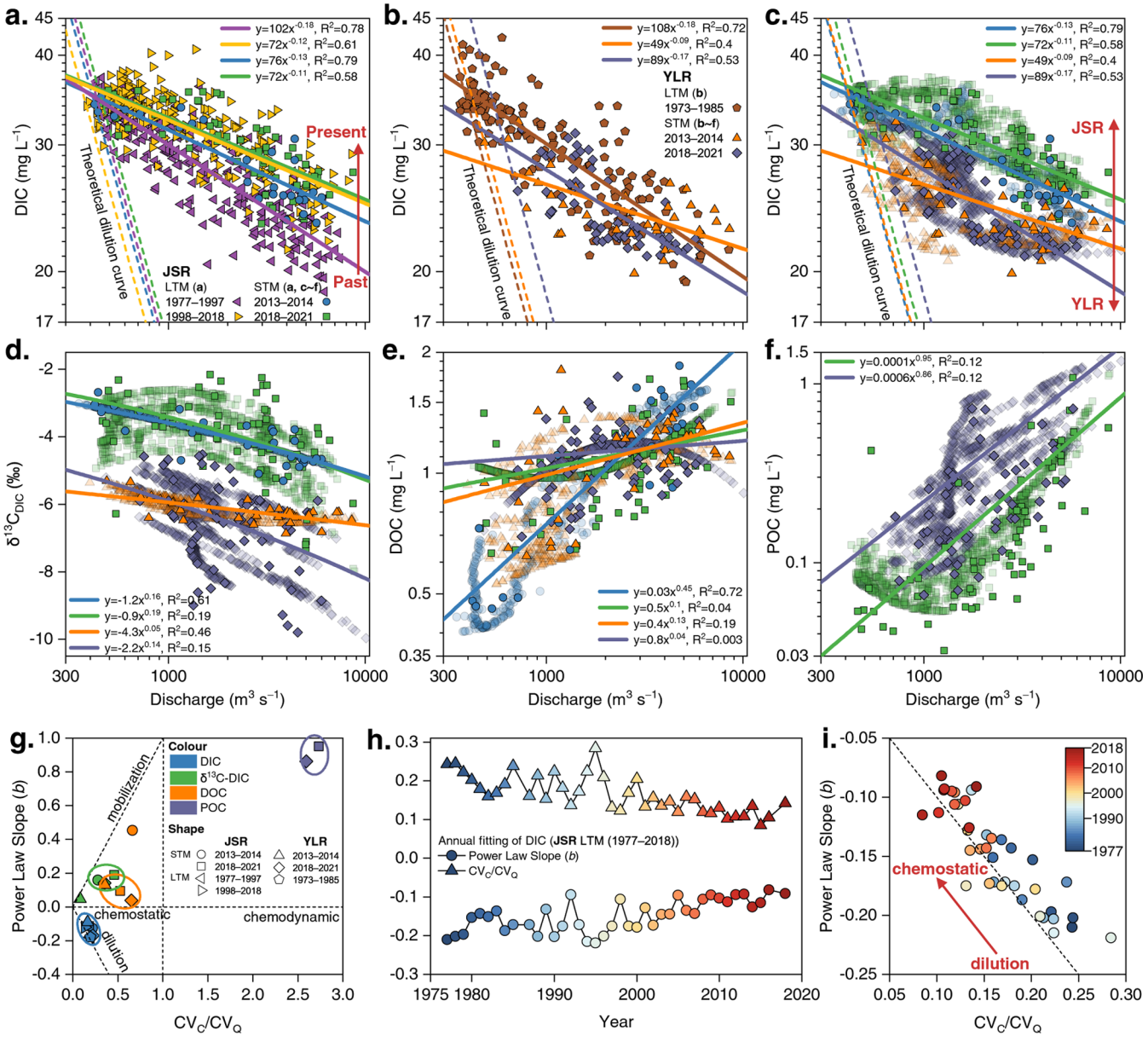

Figure 5. Concentration−discharge (C−Q) patterns. (a) Long-term measurements (LTMs) and short-term measurements (STMs) of DIC concentration in the Jinsha River (JSR). (b) LTMs and STMs of DIC concentration in the Yalong River (YLR). (c) STMs of DIC, (d) $\delta^{13}C_{DIC}$, (e) DOC, and (f) POC in the JSR and YLR, with nontransparent symbols showing the STM data and translucent symbols showing LOADEST-modeled results. Power law fitting was performed for the STM data only. The theoretical dilution curves show the variations of DIC concentrations diluted with pure water. (g) Plots of power law slope (b) versus CV_C/CV_Q for the LTM and STM. (h) Temporal evolution of annual results of the power law slope (b) and CV_C/CV_Q for the LTM of DIC in the JSR. (i) Power law slope (b) versus CV_C/CV_Q for the LTM of DIC in the JSR.

(Figures 1c and 4). The occasional spikes of DOC and POC concentrations observed during the dry season can be attributed to the effects of damming.

4.2. Long-Term DIC Response to Climate Warming. The LTM data set allows us to investigate the drivers of long-term changes in DIC concentrations and fluxes that occur alongside a progressive rise in air temperature and precipitation. Prior studies of the rivers in the headwater region of the JSR revealed a positive relationship between permafrost thawing and riverine DIC and DOC fluxes with increasing temperature.[11,15] In the JSR, both the C_{am} and C_{dwm} of DIC were strongly correlated with basin-averaged air temperature ($R^2 = 0.52$, $p < 0.01$ and $R^2 = 0.49$, $p < 0.01$, respectively) but not with basin-averaged precipitation and runoff (Figure S5; for the YLR, Figure S6). The C_{dwm} of DIC increased by 2.3 mg L^{-1} for each degree Celsius of warming (Figure S5). The DIC flux in the LTM data was estimated by combining the C_{dwm} of the DIC and runoff. In the JSR, the DIC flux (F) and the DIC flux calculated at average runoff (F_{avgR}) were significantly correlated with basin-averaged temperature ($R^2 = 0.2$, $p < 0.01$ and $R^2 = 0.49$, $p < 0.01$, respectively) (Figure S5). Due to the role of runoff in the flux calculation, the DIC flux (F) was also significantly correlated with basin-averaged precipitation ($R^2 = 0.7$, $p < 0.01$) and runoff ($R^2 = 0.76$, $p < 0.01$) (Figure S5). Increasing temperatures were accompanied by slight increases in precipitation and runoff. The DIC flux (F) thus had a temperature sensitivity different from the C_{dwm}, with an

https://doi.org/10.1021/acs.est.3c06777
Environ. Sci. Technol. 2024, 58, 7032−7044

increase of 0.67 t km^{-2} yr^{-1} for each degree Celsius of warming (Figure S5).

The decadal increase in DIC flux can be driven by increasing discharge or by increasing DIC concentration. Here, we find that the increase in DIC flux (F) (by 110%) was predominantly driven by increasing C_{dwm} (by 35%; MK: p = 0.000) rather than increasing runoff (unsubstantial increase; MK: p = 0.353). The DIC flux calculated at average runoff (F_{avgR}) can provide insights into a changing relationship between export and discharge,[6] and it also increased in the JSR (MK: p = 0.000) (Figure 2d). Hence, some processes must increase DIC concentrations for a given runoff. In addition, the $C-Q$ relationships of DIC evolved over time in the JSR, contrasting the no observable variation in the YLR (Figure 5a,b). The coefficient b and CV_C/CV_Q values of $C-Q$ relationships in the JSR showed a gradual and systematic approach to zero over the period from 1977 to 2018 (Figure 5h), indicating increasingly chemostatic behavior (Figure 5i).[52] The increasing DIC export from the JSR is probably linked to the increasing chemostasis that seems to be evoked by internal modifications within the JSR basin, such as enhanced rock weathering and soil respiration, rather than only hydrologic changes.

We hypothesized that the changes in temperature, precipitation, DIC concentration, and runoff contributed to the increase in the DIC flux (F). In an attempt to explicitly quantify the contributions of each of the changes of these variables to the increase in DIC flux (F) in the JSR, we calculated the slope change ratios of cumulative quantities of variables (Supporting Text S4). The slope change ratios between the periods 1977−1997 and 1998−2018 were 69% for basin-averaged temperature, 7% for basin-averaged precipitation, 7% for runoff, 20% for C_{dwm}, and 28% for DIC flux (F) (Figure S7 and Table S7). The relative slope change ratios suggest that the changes in basin-averaged temperature and precipitation contributed 90 and 10% to the increase in DIC flux (F), respectively (Figure S8 and Table S7). In turn, the changes in C_{dwm} and runoff contributed 75 and 25% to the increase in DIC flux (F), respectively (Figure S8 and Table S7). These explicit relationships suggest that the increases in DIC concentration and flux were primarily driven by increasing temperatures, whereas increasing precipitation rates were a relatively minor contribution.

Whereas the YLR basin has similarly experienced warming, it does not show long-term increases in DIC concentrations and fluxes as observed in the JSR, possibly due to a comparatively low cover of continuous permafrost and to a limited exposure of evaporite deposits in the YLR headwaters (Figure 1a).[43,44] In addition, the warming rates in the YLR basin were generally lower than those in the JSR basin due to its lower elevation. The slight decrease in DIC concentrations in the YLR may be attributed to the effect of reservoir regulation and the dilution of increasing discharge. Because of the larger multiyear mean monthly discharge of the STM than that of the LTM (Figure 3d), the DIC flux of the STM in the YLR does not show a decrease but remains at the same level as that of the LTM (Figure S2d).

Because no long-term records of riverine DOC and POC fluxes exist in the JSR and YLR or even in the QTP and China,[75] we could not analyze the impacts of warming on their long-term trends. However, prior studies have shown warming-driven increases in DOC releases in the central permafrost regions of the QTP on seasonal time scales.[15,42] In fact, SOC stored in permafrost is expected to become more reactive during warming and the released DOC and POC represent an important potential carbon source that can offset the regional carbon sink.[13,14,21,22] Therefore, climate warming could potentially alter the riverine export of DOC and POC in the QTP. Because DIC concentrations are more than ten times higher than DOC and POC concentrations in the JSR, the DIC flux constitutes predominantly the riverine total carbon flux. We can therefore conclude that riverine total carbon export from the JSR is escalating with climate warming.

4.3. Implications for the Carbon Cycle. Escalating DIC concentrations and fluxes of the JSR occurring alongside progressively rising air temperature suggest the direct or indirect influence of warming on the net production of geogenic and biogenic DIC (Figure S8). Chemical weathering could respond to warming directly due to the increase in dissolution kinetics or indirectly due to the additional minerals exposed through permafrost thaw.[57,66,76,77] In particular, carbonate weathering intensity is positively correlated with land temperature when the temperature is below 10 °C, with maximum intensity between 10 and 15 °C.[78] Silicate weathering rate is limited by the kinetics of weathering reactions when weathering materials are abundant[57,77] and, therefore, is expected to be positively sensitive to warming in the high-elevation mountains of the QTP, where basin-wide erosion rates are high.[79,80]

The increased DIC fluxes could arise from the increased chemical weathering driven by increased exposure of minerals due to glacier recession, snowmelt, permafrost thaw, rainfall, and increased erosion through strengthened precipitation events (Figure S8).[34,66,80] In particular, permafrost thawing and the resulting deepening of the active layer and flow path can expose unweathered mineral surfaces, prolong water residence times, and enhance mixing with mineral-rich subsurface flow and groundwater.[8,12] In addition, root respiration of plants and microbial respiration of soil organic matter are generally thought to increase under warmer temperatures.[8,22,81] Soil respiration produced CO_2 can be an important direct contributor of DIC,[7] and increasing CO_2 from soil respiration and organic acids with rising soil water availability could promote mineral weathering reactions.[57,66]

The increased DIC fluxes may also partly result from the increased dissolution of evaporite carbonates and hydrogen carbonates (e.g., Trona ($Na_2CO_3{\cdot}NaHCO_3{\cdot}2H_2O$) and Northupite ($Na_2CO_3{\cdot}MgCO_3{\cdot}NaCl$)) that are distributed in the headwater region of the JSR,[44,80] and increased sulfide oxidation coupled to carbonate dissolution.[80,82] In the JSR basin, the increase of Ca^{2+} + Mg^{2+} is accompanied by the increases of both DIC and SO_4^{2-} (Figure S9a). Increased Ca^{2+} + Mg^{2+} concentration and electrical conductivity with decreased DIC/(Ca^{2+} + Mg^{2+}) ratios suggest an increased contribution of evaporite dissolution and/or sulfide oxidation coupled to carbonate weathering to Ca^{2+} + Mg^{2+} (Figure S9b).[80,83] Evaporite and sulfide weathering can be accelerated with increasing temperature and greater mineral supply resulting from enhanced erosion and changes in the flow path driven by warming.[12,66,76]

In contrast to silicate and carbonate weathering, sulfide oxidation releases CO_2 into the atmosphere by supplying sulfuric acids to consume alkalinity.[66,80,82] Carbonate weathering and sulfide oxidation tend to be more sensitive to erosion and mineral exposure than silicate weathering at high erosion rates.[66,80,84] Therefore, where exposure of minerals by

https://doi.org/10.1021/acs.est.3c06777
Environ. Sci. Technol. 2024, 58, 7032−7044

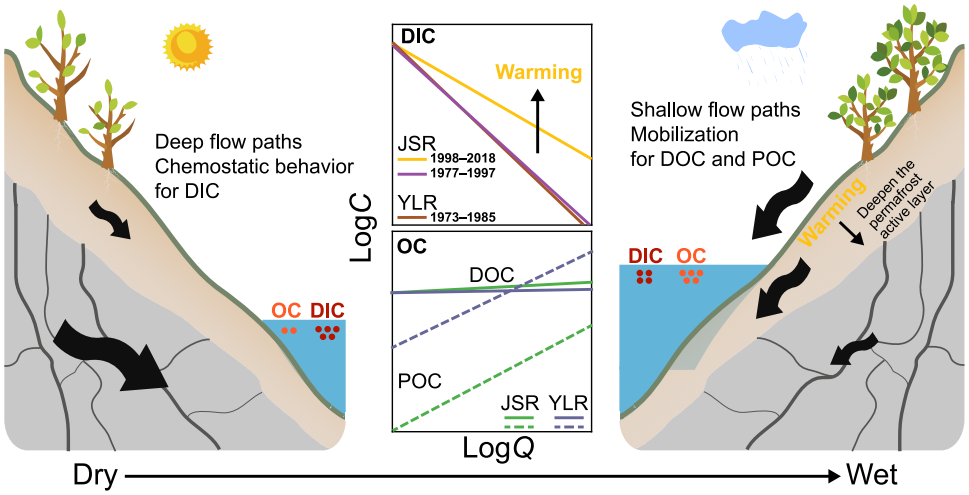

Figure 6. Schematic depicting the hypothesized effects of seasonal flow path variability and decadal climate warming on the concentration−discharge ($C-Q$) relationship. The schematic lines showing the relationships of DIC, DOC, and POC concentrations with discharge are from Figure 5. The purple and yellow lines represent the long-term measurements (LTMs) of DIC in the Jinsha River (JSR) during 1977−1997 and 1998−2018, respectively, and the brown line represents the LTMs of DIC in the Yalong River (YLR) during 1973−1985. The green lines represent the short-term measurements (STMs) of DOC (solid line) and POC (dotted line) in the JSR during 2018−2021, and the blue lines represent the STMs of DOC (solid line) and POC (dotted line) in the YLR during 2018−2021. The JSR and YLR basins have arid and humid climatic conditions, respectively. Climate warming enhanced the chemostatic behavior of DIC in the JSR by driving soil respiration and mineral weathering in high-elevation headwater regions.

permafrost thaw is a major process for enhanced weathering under a warming climate, carbonates and sulfides are expected to contribute disproportionally to DIC fluxes due to their faster dissolution kinetics and additional mineral supplies. Silicate weathering acts as a long-term sink for atmospheric CO_2, while carbonate weathering acts CO_2-neutral beyond the calcium carbonate compensation time ($\sim 10^3-10^4$ years), and sulfide oxidation acts as a source for atmospheric CO_2 until the sulfate is reduced to sulfides in marine sediments (on time scales of $\sim 10^6-10^7$ years).[66,80,82,85] Therefore, warming and permafrost thawing could shift the regional inorganic carbon budget of chemical weathering and the relationship between chemical weathering and the carbon cycle.

Seasonal variations in $\delta^{13}C_{DIC}$ values, as well as in DIC, DOC, and POC concentrations, support the Shallow and Deep Hypothesis, which proposes that changes in the contributions of shallow soil water and deeper groundwater flow paths to runoff determine the $C-Q$ patterns of these compounds (Figure 6).[7,18,65] Elevated DIC concentration and $\delta^{13}C_{DIC}$, coupled with reduced OC concentrations, were observed during periods of low discharge, suggesting a predominance of DIC-enriched and OC-poor groundwater in river discharge. In turn, at high discharge, DIC-poor and OC-enriched shallow soil water appeared to dominate river discharge due to intense rainfall and biological activity. Such intra-annual patterns of carbon dynamics highlight the importance of land-river connectivity via subsurface flow paths.[86] Based on this pattern, warming changed the $C-Q$ relationship of DIC in the JSR basin, resulting in increasingly chemostatic behavior of DIC and more DIC export under a given discharge (Figure 6). The transition of DIC export regimes from dilution in the 1970s and 1980s to chemostasis in the 2010s suggests a shift in concentration gradients within the shallow and deep subsurface zones, as can be inferred from the Shallow and Deep Hypothesis.[7,18,65] Although direct measurements are lacking, it is possible that the DIC concentrations in the shallow soil water have increased during the warmer years of the later decade, eventually becoming comparable to those in deeper zones such that riverine DIC concentrations become similar under different discharge regimes (chemostasis). This hypothesis is further supported by observations of lighter $\delta^{13}C_{DIC}$ signatures under higher discharge in the monsoon season, indicating predominant sourcing of biogenic DIC from shallow soils under wet conditions.

Given the more rapid warming in the QTP compared to low-land places, the rivers in the QTP can offer early glimpses of the impacts of climate change on fluvial biogeochemistry. We advocate for establishing monitoring stations for rivers in the high-elevation mountain regions as sentinel sites to record long-term alterations of fluvial biogeochemistry in response to a changing climate in addition to observing hydrometeorological variables.

■ ASSOCIATED CONTENT

Supporting Information

The Supporting Information is available free of charge at https://pubs.acs.org/doi/10.1021/acs.est.3c06777.

Details regarding long-term measurement data set and data reliability (Text S1); hydrometeorological data sources (Text S2); linear trend evaluation (Text S3); analyses of cumulative anomaly and slope change ratio of cumulative quantity (Text S4); metrics defining the export regime (Text S5); long-term trend of electrical conductivity (Figure S1); long-term trends of variables in the Yalong River Basin (Figure S2); annual trends of meteorological variables measured at four weather stations (Figure S3) and of hydrologic variables measured at four gauging stations (Figure S4); DIC concentration and flux versus hydrometeorological variables in the Jinsha River Basin (Figure S5) and in the Yalong River Basin (Figure S6); variations of cumulative variable anomalies and cumulative variables (Figure S7); flowchart of attributing the increased DIC concentration and flux to climate change (Figure S8);

https://doi.org/10.1021/acs.est.3c06777
Environ. Sci. Technol. 2024, 58, 7032−7044

DIC versus Ca^{2+} + Mg^{2+} and DIC/(Ca^{2+} + Mg^{2+}) versus electrical conductivity (Figure S9); annual data of long-term measurements and short-term measurements (Table S1); short-term measurements of DIC, $\delta^{13}C_{DIC}$, DOC, and POC (Table S2); multiple linear stepwise regression models used to infer the lacking data of alkalinity concentrations (Table S3); linear trend evaluation for the variables in the Jinsha River and Yalong River Basins (Table S4); LOADEST models selected for flux calculations (Table S5); monthly data for different periods (Table S6); and quantifying the contributions of the changes in variables to the increase in DIC flux (Table S7) (PDF)

AUTHOR INFORMATION

Corresponding Author

Si-Liang Li − *Institute of Surface-Earth System Sciences, School of Earth System Science, Tianjin University, Tianjin 300072, China;* orcid.org/0000-0002-0295-9675; Email: siliang.li@tju.edu.cn

Authors

Sen Xu − *Institute of Surface-Earth System Sciences, School of Earth System Science, Tianjin University, Tianjin 300072, China;* orcid.org/0000-0002-7290-8574

Aaron Bufe − *Department of Earth and Environmental Sciences, Ludwig-Maximilians-Universität München, Munich 80333, Germany*

Marcus Klaus − *Department of Forest Ecology and Management, Swedish University of Agricultural Sciences, Umeå 90736, Sweden*

Jun Zhong − *Institute of Surface-Earth System Sciences, School of Earth System Science, Tianjin University, Tianjin 300072, China*

Hang Wen − *Institute of Surface-Earth System Sciences, School of Earth System Science, Tianjin University, Tianjin 300072, China*

Shuai Chen − *Department of Geography, The University of Hong Kong, Hong Kong 999077, China*

Li Li − *Department of Civil & Environmental Engineering, The Pennsylvania State University, University Park, Pennsylvania 16802, United States;* orcid.org/0000-0002-1641-3710

Complete contact information is available at: https://pubs.acs.org/10.1021/acs.est.3c06777

Author Contributions

The manuscript was written through the contribution of all authors. All authors have given approval to the final version of the manuscript.

Notes

The authors declare no competing financial interest.

ACKNOWLEDGMENTS

This research is co-supported financially by the National Natural Science Foundation of China (Grant Nos. 41925002 and 42303058) and the Second Tibetan Plateau Scientific Expedition and Research (2019QZKK0707).

REFERENCES

(1) Battin, T. J.; Lauerwald, R.; Bernhardt, E. S.; Bertuzzo, E.; Gener, L. G.; Hall, R. O., Jr.; Hotchkiss, E. R.; Maavara, T.; Pavelsky, T. M.; Ran, L.; Raymond, P.; Rosentreter, J. A.; Regnier, P. River ecosystem metabolism and carbon biogeochemistry in a changing world. *Nature* **2023**, *613* (7944), 449−459.

(2) Galy, V.; Peucker-Ehrenbrink, B.; Eglinton, T. Global carbon export from the terrestrial biosphere controlled by erosion. *Nature* **2015**, *521* (7551), 204−207.

(3) Battin, T. J.; Luyssaert, S.; Kaplan, L. A.; Aufdenkampe, A. K.; Richter, A.; Tranvik, L. J. The boundless carbon cycle. *Nat. Geosci.* **2009**, *2* (9), 598−600.

(4) Regnier, P.; Resplandy, L.; Najjar, R. G.; Ciais, P. The land-to-ocean loops of the global carbon cycle. *Nature* **2022**, *603* (7901), 401−410.

(5) Cole, J. J.; Prairie, Y. T.; Caraco, N. F.; McDowell, W. H.; Tranvik, L. J.; Striegl, R. G.; Duarte, C. M.; Kortelainen, P.; Downing, J. A.; Middelburg, J. J.; Melack, J. Plumbing the Global Carbon Cycle: Integrating Inland Waters into the Terrestrial Carbon Budget. *Ecosystems* **2007**, *10* (1), 172−185.

(6) Raymond, P. A.; Oh, N. H.; Turner, R. E.; Broussard, W. Anthropogenically enhanced fluxes of water and carbon from the Mississippi River. *Nature* **2008**, *451* (7177), 449−452.

(7) Stewart, B.; Zhi, W.; Sadayappan, K.; Sterle, G.; Harpold, A.; Li, L. Soil CO_2 Controls Short-Term Variation but Climate Regulates Long-Term Mean of Riverine Inorganic Carbon. *Global Biogeochem. Cycles* **2022**, *36* (8), No. e2022GB007351.

(8) Drake, T. W.; Tank, S. E.; Zhulidov, A. V.; Holmes, R. M.; Gurtovaya, T.; Spencer, R. G. M. Increasing Alkalinity Export from Large Russian Arctic Rivers. *Environ. Sci. Technol.* **2018**, *52* (15), 8302−8308.

(9) Tank, S. E.; Striegl, R. G.; McClelland, J. W.; Kokelj, S. V. Multi-decadal increases in dissolved organic carbon and alkalinity flux from the Mackenzie drainage basin to the Arctic Ocean. *Environ. Res. Lett.* **2016**, *11* (5), No. 054015.

(10) Tank, S. E.; McClelland, J. W.; Spencer, R. G. M.; Shiklomanov, A. I.; Suslova, A.; Moatar, F.; Amon, R. M. W.; Cooper, L. W.; Elias, G.; Gordeev, V. V.; Guay, C.; Gurtovaya, T. Y.; Kosmenko, L. S.; Mutter, E. A.; Peterson, B. J.; Peucker-Ehrenbrink, B.; Raymond, P. A.; Schuster, P. F.; Scott, L.; Staples, R.; Striegl, R. G.; Tretiakov, M.; Zhulidov, A. V.; Zimov, N.; Zimov, S.; Holmes, R. M. Recent trends in the chemistry of major northern rivers signal widespread Arctic change. *Nat. Geosci.* **2023**, *16* (9), 789−796.

(11) Song, C.; Wang, G.; Mao, T.; Huang, K.; Sun, X.; Hu, Z.; Chang, R.; Chen, X.; Raymond, P. A. Spatiotemporal Variability and Sources of DIC in Permafrost Catchments of the Yangtze River Source Region: Insights From Stable Carbon Isotope and Water Chemistry. *Water Resour. Res.* **2020**, *56* (1), No. e2019WR025343.

(12) Zolkos, S.; Tank, S. E.; Kokelj, S. V. Mineral Weathering and the Permafrost Carbon-Climate Feedback. *Geophys. Res. Lett.* **2018**, *45* (18), 9623−9632.

(13) Mu, C. C.; Abbott, B. W.; Wu, X. D.; Zhao, Q.; Wang, H. J.; Su, H.; Wang, S. F.; Gao, T. G.; Guo, H.; Peng, X. Q.; Zhang, T. J. Thaw Depth Determines Dissolved Organic Carbon Concentration and Biodegradability on the Northern Qinghai-Tibetan Plateau. *Geophys. Res. Lett.* **2017**, *44* (18), 9389−9399.

(14) Schuur, E. A. G.; McGuire, A. D.; Schadel, C.; Grosse, G.; Harden, J. W.; Hayes, D. J.; Hugelius, G.; Koven, C. D.; Kuhry, P.; Lawrence, D. M.; Natali, S. M.; Olefeldt, D.; Romanovsky, V. E.; Schaefer, K.; Turetsky, M. R.; Treat, C. C.; Vonk, J. E. Climate change and the permafrost carbon feedback. *Nature* **2015**, *520* (7546), 171−179.

(15) Song, C.; Wang, G.; Mao, T.; Chen, X.; Huang, K.; Sun, X.; Hu, Z. Importance of active layer freeze-thaw cycles on the riverine dissolved carbon export on the Qinghai-Tibet Plateau permafrost region. *PeerJ* **2019**, *7*, No. e7146.

(16) Rehn, L.; Sponseller, R. A.; Laudon, H.; Wallin, M. B. Long-term changes in dissolved inorganic carbon across boreal streams caused by altered hydrology. *Limnol. Oceanogr.* **2023**, *68* (2), 409−423.

(17) Kaushal, S. S.; Likens, G. E.; Utz, R. M.; Pace, M. L.; Grese, M.; Yepsen, M. Increased River Alkalinization in the Eastern US. *Environ. Sci. Technol.* **2013**, *47* (18), 10302−10311.
(18) Kerins, D.; Li, L. High Dissolved Carbon Concentration in Arid Rocky Mountain Streams. *Environ. Sci. Technol.* **2023**, *57* (11), 4656−4667.
(19) Regnier, P.; Friedlingstein, P.; Ciais, P.; Mackenzie, F. T.; Gruber, N.; Janssens, I. A.; Laruelle, G. G.; Lauerwald, R.; Luyssaert, S.; Andersson, A. J.; Arndt, S.; Arnosti, C.; Borges, A. V.; Dale, A. W.; Gallego-Sala, A.; Goddéris, Y.; Goossens, N.; Hartmann, J.; Heinze, C.; Ilyina, T.; Joos, F.; LaRowe, D. E.; Leifeld, J.; Meysman, F. J. R.; Munhoven, G.; Raymond, P. A.; Spahni, R.; Suntharalingam, P.; Thullner, M. Anthropogenic perturbation of the carbon fluxes from land to ocean. *Nat. Geosci.* **2013**, *6* (8), 597−607.
(20) Nai, H.; Zhong, J.; Yi, Y.; Lai, M.; He, D.; Dittmar, T.; Liu, C. Q.; Li, S. L.; Xu, S. Anthropogenic Disturbance Stimulates the Export of Dissolved Organic Carbon to Rivers on the Tibetan Plateau. *Environ. Sci. Technol.* **2023**, *57* (25), 9214−9223.
(21) Drake, T. W.; Wickland, K. P.; Spencer, R. G. M.; McKnight, D. M.; Striegl, R. G. Ancient low-molecular-weight organic acids in permafrost fuel rapid carbon dioxide production upon thaw. *Proc. Natl. Acad. Sci. U.S.A.* **2015**, *112* (45), 13946−13951.
(22) Wang, T.; Yang, D.; Yang, Y.; Piao, S.; Li, X.; Cheng, G.; Fu, B. Permafrost thawing puts the frozen carbon at risk over the Tibetan Plateau. *Sci. Adv.* **2020**, *6* (19), No. eaaz3513.
(23) Yao, T.; Bolch, T.; Chen, D.; Gao, J.; Immerzeel, W.; Piao, S.; Su, F.; Thompson, L.; Wada, Y.; Wang, L.; Wang, T.; Wu, G.; Xu, B.; Yang, W.; Zhang, G.; Zhao, P. The imbalance of the Asian water tower. *Nat. Rev. Earth Environ.* **2022**, *3* (10), 618−632.
(24) Zhang, G.; Bolch, T.; Chen, W.; Cretaux, J. F. Comprehensive estimation of lake volume changes on the Tibetan Plateau during 1976−2019 and basin-wide glacier contribution. *Sci. Total Environ.* **2021**, *772*, No. 145463.
(25) Yao, T.; Xue, Y.; Chen, D.; Chen, F.; Thompson, L.; Cui, P.; Koike, T.; Lau, W. K. M.; Lettenmaier, D.; Mosbrugger, V.; Zhang, R.; Xu, B.; Dozier, J.; Gillespie, T.; Gu, Y.; Kang, S.; Piao, S.; Sugimoto, S.; Ueno, K.; Wang, L.; Wang, W.; Zhang, F.; Sheng, Y.; Guo, W.; Ailikun; Yang, X.; Ma, Y.; Shen, S. S. P.; Su, Z.; Chen, F.; Liang, S.; Liu, Y.; Singh, V. P.; Yang, K.; Yang, D.; Zhao, X.; Qian, Y.; Zhang, Y.; Li, Q. Recent Third Pole's Rapid Warming Accompanies Cryospheric Melt and Water Cycle Intensification and Interactions between Monsoon and Environment: Multidisciplinary Approach with Observations, Modeling, and Analysis. *Bull. Am. Meteorol. Soc.* **2019**, *100* (3), 423−444.
(26) Zhi, W.; Williams, K. H.; Carroll, R. W. H.; Brown, W.; Dong, W.; Kerins, D.; Li, L. Significant stream chemistry response to temperature variations in a high-elevation mountain watershed. *Commun. Earth Environ.* **2020**, *1* (1), No. 43.
(27) Immerzeel, W. W.; Lutz, A. F.; Andrade, M.; Bahl, A.; Biemans, H.; Bolch, T.; Hyde, S.; Brumby, S.; Davies, B. J.; Elmore, A. C.; Emmer, A.; Feng, M.; Fernandez, A.; Haritashya, U.; Kargel, J. S.; Koppes, M.; Kraaijenbrink, P. D. A.; Kulkarni, A. V.; Mayewski, P. A.; Nepal, S.; Pacheco, P.; Painter, T. H.; Pellicciotti, F.; Rajaram, H.; Rupper, S.; Sinisalo, A.; Shrestha, A. B.; Viviroli, D.; Wada, Y.; Xiao, C.; Yao, T.; Baillie, J. E. M. Importance and vulnerability of the world's water towers. *Nature* **2020**, *577* (7790), 364−369.
(28) Yang, K.; Wu, H.; Qin, J.; Lin, C.; Tang, W.; Chen, Y. Recent climate changes over the Tibetan Plateau and their impacts on energy and water cycle: A review. *Global Planet. Change* **2014**, *112*, 79−91.
(29) Chen, H.; Zhu, Q.; Peng, C.; Wu, N.; Wang, Y.; Fang, X.; Gao, Y.; Zhu, D.; Yang, G.; Tian, J.; Kang, X.; Piao, S.; Ouyang, H.; Xiang, W.; Luo, Z.; Jiang, H.; Song, X.; Zhang, Y.; Yu, G.; Zhao, X.; Gong, P.; Yao, T.; Wu, J. The impacts of climate change and human activities on biogeochemical cycles on the Qinghai-Tibetan Plateau. *Global Change Biol.* **2013**, *19* (10), 2940−2955.
(30) Brun, F.; Berthier, E.; Wagnon, P.; Kääb, A.; Treichler, D. A spatially resolved estimate of High Mountain Asia glacier mass balances from 2000 to 2016. *Nat. Geosci.* **2017**, *10* (9), 668−673.
(31) Cheng, G.; Wu, T. Responses of permafrost to climate change and their environmental significance, Qinghai-Tibet Plateau. *J. Geophys. Res.* **2007**, *112*, No. F02S03.
(32) Zhang, G.; Yao, T.; Xie, H.; Yang, K.; Zhu, L.; Shum, C. K.; Bolch, T.; Yi, S.; Allen, S.; Jiang, L.; Chen, W.; Ke, C. Response of Tibetan Plateau lakes to climate change: Trends, patterns, and mechanisms. *Earth-Sci. Rev.* **2020**, *208*, No. 103269.
(33) Niu, F.; Lin, Z.; Liu, H.; Lu, J. Characteristics of thermokarst lakes and their influence on permafrost in Qinghai−Tibet Plateau. *Geomorphology* **2011**, *132* (3−4), 222−233.
(34) Li, D.; Li, Z.; Zhou, Y.; Lu, X. Substantial Increases in the Water and Sediment Fluxes in the Headwater Region of the Tibetan Plateau in Response to Global Warming. *Geophys. Res. Lett.* **2020**, *47* (11), No. e2020GL087745.
(35) Li, D.; Lu, X.; Overeem, I.; Walling, D. E.; Syvitski, J.; Kettner, A. J.; Bookhagen, B.; Zhou, Y.; Zhang, T. Exceptional increases in fluvial sediment fluxes in a warmer and wetter High Mountain Asia. *Science* **2021**, *374* (6567), 599−603.
(36) Mu, C.; Mu, M.; Wu, X.; Jia, L.; Fan, C.; Peng, X.; Ping, C. L.; Wu, Q.; Xiao, C.; Liu, J. High carbon emissions from thermokarst lakes and their determinants in the Tibet Plateau. *Global Change Biol.* **2023**, *29* (10), 2732−2745.
(37) Wang, P.; Huang, Q.; Liu, S.; Liu, Y.; Li, Z.; Pozdniakov, S. P.; Wang, T.; Kazak, E. S.; Frolova, N. L.; Gabysheva, O. I.; Zhang, J.; Bai, B.; Yu, J.; Min, L.; Shpakova, R. N.; Hao, L.; Gabyshev, V. A. Climate warming enhances chemical weathering in permafrost-dominated eastern Siberia. *Sci. Total Environ.* **2024**, *906*, No. 167367.
(38) Zhong, J.; Li, S.-L.; Zhu, X.; Liu, J.; Xu, S.; Xu, S.; Liu, C.-Q. Dynamics and fluxes of dissolved carbon under short-term climate variabilities in headwaters of the Changjiang River, draining the Qinghai-Tibet Plateau. *J. Hydrol.* **2021**, *596*, No. 126128.
(39) You, X.; Li, X.; Sillanpää, M.; Wang, R.; Wu, C.; Xu, Q. Export of Dissolved Organic Carbon from the Source Region of Yangtze River in the Tibetan Plateau. *Sustainability* **2022**, *14* (4), 2441.
(40) Wang, X.; Liu, T.; Wang, L.; Liu, Z.; Zhu, E.; Wang, S.; Cai, Y.; Zhu, S.; Feng, X. Spatial-temporal variations in riverine carbon strongly influenced by local hydrological events in an alpine headwater stream. *Biogeosciences* **2021**, *18*, 3015−3028.
(41) Qu, B.; Sillanpaa, M.; Kang, S.; Yan, F.; Li, Z.; Zhang, H.; Li, C. Export of dissolved carbonaceous and nitrogenous substances in rivers of the "Water Tower of Asia". *J. Environ. Sci.* **2018**, *65*, 53−61.
(42) Qu, B.; Sillanpaa, M.; Li, C.; Kang, S.; Stubbins, A.; Yan, F.; Aho, K. S.; Zhou, F.; Raymond, P. A. Aged dissolved organic carbon exported from rivers of the Tibetan Plateau. *PLoS One* **2017**, *12* (5), No. e0178166.
(43) Obu, J.; Westermann, S.; Kääb, A.; Bartsch, A. *Permafrost Extent and Ground Temperature Map, 2000−2016, Northern Hemisphere Permafrost*, PANGAEA, 2018. https://apgc.awi.de/dataset/pex.
(44) Zheng, M.; Liu, X. Hydrochemistry and Minerals Assemblages of Salt Lakes in the Qinghai-Tibet Plateau, China. *Acta Geol. Sin.* **2010**, *84* (11), 1585−1600.
(45) Chen, B.-B.; Li, S.-L.; Pogge von Strandmann, P. A. E.; Wilson, D. J.; Zhong, J.; Ma, T.-T.; Sun, J.; Liu, C.-Q. Behaviour of Sr, Ca, and Mg isotopes under variable hydrological conditions in high-relief large river systems. *Geochim. Cosmochim. Acta* **2023**, *343*, 142−160.
(46) Chen, J.; Wang, F.; Xia, X.; Zhang, L. Major element chemistry of the Changjiang (Yangtze River). *Chem. Geol.* **2002**, *187* (3), 231−255.
(47) Ran, L.; Lu, X. X.; Liu, S. Dynamics of riverine CO_2 in the Yangtze River fluvial network and their implications for carbon evasion. *Biogeosciences* **2017**, *14* (8), 2183−2198.
(48) Lewis, E. R.; Wallace, D. W. R. *Program Developed for CO_2 System Calculations*; ORNL/CDIAC-105, Carbon dioxide Information Analysis Center; Oak Ridge National Laboratory: Oak Ridge, TN, USA, 1998.
(49) Jones, J. B.; Stanley, E. H.; Mulholland, P. J. Long-term decline in carbon dioxide supersaturation in rivers across the contiguous United States. *Geophys. Res. Lett.* **2003**, *30* (10), No. 1495.

https://doi.org/10.1021/acs.est.3c06777
Environ. Sci. Technol. 2024, 58, 7032−7044

(50) Hamed, K. H.; Rao, A. R. A modified Mann-Kendall trend test for autocorrelated data. *J. Hydrol.* **1998**, *204* (1−4), 182−196.
(51) Wang, S.; Yan, M.; Yan, Y.; Shi, C.; He, L. Contributions of climate change and human activities to the changes in runoff increment in different sections of the Yellow River. *Quat. Int.* **2012**, *282*, 66−77.
(52) Musolff, A.; Schmidt, C.; Selle, B.; Fleckenstein, J. H. Catchment controls on solute export. *Adv. Water Resour.* **2015**, *86*, 133−146.
(53) Godsey, S. E.; Kirchner, J. W.; Clow, D. W. Concentration-discharge relationships reflect chemostatic characteristics of US catchments. *Hydrol. Processes* **2009**, *23* (13), 1844−1864.
(54) Pörtner, H.-O.; Roberts, D. C.; Masson-Delmotte, V.; Zhai, P.; Tignor, M.; Poloczanska, E.; Weyer, N. *The Ocean and Cryosphere in a Changing Climate*; IPCC Special Report on the Ocean and Cryosphere in a Changing Climate, 2019; Vol. *1155*.
(55) Zhang, W.; Zhou, T.; Zhang, L. Wetting and greening Tibetan Plateau in early summer in recent decades. *J. Geophys. Res.: Atmos.* **2017**, *122* (11), 5808−5822.
(56) Zhong, J.; Li, S.; Tao, F.; Yue, F.; Liu, C. Q. Sensitivity of chemical weathering and dissolved carbon dynamics to hydrological conditions in a typical karst river. *Sci. Rep.* **2017**, *7*, No. 42944.
(57) Tipper, E. T.; Bickle, M. J.; Galy, A.; West, A. J.; Pomiès, C.; Chapman, H. J. The short term climatic sensitivity of carbonate and silicate weathering fluxes: Insight from seasonal variations in river chemistry. *Geochim. Cosmochim. Acta* **2006**, *70* (11), 2737−2754.
(58) Wen, H.; Sullivan, P. L.; Billings, S. A.; Ajami, H.; Cueva, A.; Flores, A.; Hirmas, D. R.; Koop, A. N.; Murenbeeld, K.; Zhang, X.; Li, L. From Soils to Streams: Connecting Terrestrial Carbon Transformation, Chemical Weathering, and Solute Export Across Hydrological Regimes. *Water Resour. Res.* **2022**, *58* (7), No. e2022WR032314.
(59) Marwick, T. R.; Tamooh, F.; Teodoru, C. R.; Borges, A. V.; Darchambeau, F.; Bouillon, S. The age of river-transported carbon: A global perspective. *Global Biogeochem. Cycles* **2015**, *29* (2), 122−137.
(60) Lin, G.; Ehleringer, J. R. Carbon isotopic fractionation does not occur during dark respiration in C3 and C4 plants. *Plant Physiol.* **1997**, *114* (1), 391−394.
(61) Khadka, M. B.; Martin, J. B.; Jin, J. Transport of dissolved carbon and CO_2 degassing from a river system in a mixed silicate and carbonate catchment. *J. Hydrol.* **2014**, *513*, 391−402.
(62) Chen, S.; Zhong, J.; Li, C.; Liu, J.; Wang, W.; Xu, S.; Li, S.-L. Coupled effects of hydrology and temperature on temporal dynamics of dissolved carbon in the Min River, Tibetan Plateau. *J. Hydrol.* **2021**, *593*, No. 125641.
(63) Doctor, D. H.; Kendall, C.; Sebestyen, S. D.; Shanley, J. B.; Ohte, N.; Boyer, E. W. Carbon isotope fractionation of dissolved inorganic carbon (DIC) due to outgassing of carbon dioxide from a headwater stream. *Hydrol. Processes* **2008**, *22* (14), 2410−2423.
(64) Becker, J. A.; Bickle, M. J.; Galy, A.; Holland, T. J. B. Himalayan metamorphic CO_2 fluxes: Quantitative constraints from hydrothermal springs. *Earth Planet. Sci. Lett.* **2008**, *265* (3−4), 616−629.
(65) Zhi, W.; Li, L.; Dong, W.; et al. Distinct Source Water Chemistry Shapes Contrasting Concentration-Discharge Patterns. *Water Resour. Res.* **2019**, *55* (5), 4233−4251.
(66) Bufe, A.; Hovius, N.; Emberson, R.; Rugenstein, J. K. C.; Galy, A.; Hassenruck-Gudipati, H. J.; Chang, J.-M. Co-variation of silicate, carbonate and sulfide weathering drives CO_2 release with erosion. *Nat. Geosci.* **2021**, *14* (4), 211−216.
(67) Xiao, D. C.; Brantley, S. L.; Li, L. Vertical Connectivity Regulates Water Transit Time and Chemical Weathering at the Hillslope Scale. *Water Resour. Res.* **2021**, *57* (8), No. e2020WR029207.
(68) Godsey, S. E.; Hartmann, J.; Kirchner, J. W. Catchment chemostasis revisited: Water quality responds differently to variations in weather and climate. *Hydrol. Processes* **2019**, *33* (24), 3056−3069.
(69) Shih, Y. T.; Chen, P. H.; Lee, L. C.; Liao, C. S.; Jien, S. H.; Shiah, F. K.; Lee, T. Y.; Hein, T.; Zehetner, F.; Chang, C. T.; Huang, J. C. Dynamic responses of DOC and DIC transport to different flow regimes in a subtropical small mountainous river. *Hydrol. Earth Syst. Sci.* **2018**, *22* (12), 6579−6590.
(70) Hornberger, G. M.; Bencala, K. E.; Mcknight, D. M. Hydrological controls on dissolved organic carbon during snowmelt in the Snake River near Montezuma, Colorado. *Biogeochemistry* **1994**, *25* (3), 147−165.
(71) Smith, J. C.; Galy, A.; Hovius, N.; Tye, A. M.; Turowski, J. M.; Schleppi, P. Runoff-driven export of particulate organic carbon from soil in temperate forested uplands. *Earth Planet. Sci. Lett.* **2013**, *365*, 198−208.
(72) Xu, S.; Yue, F.-J.; Li, S.-L.; Ding, H.; Xu, S.; Lang, Y.-C.; Liu, C.-Q. Carbon and nitrogen isotope constraints on source and variation of particulate organic matter in high-latitude agricultural rivers, Northeast China. *J. Cleaner Prod.* **2021**, *321*, No. 128974.
(73) Vonk, J. E.; Tank, S. E.; Bowden, W. B.; Laurion, I.; Vincent, W. F.; Alekseychik, P.; Amyot, M.; Billet, M. F.; Canário, J.; Cory, R. M.; Deshpande, B. N.; Helbig, M.; Jammet, M.; Karlsson, J.; Larouche, J.; MacMillan, G.; Rautio, M.; Walter Anthony, K. M.; Wickland, K. P. Reviews and syntheses: Effects of permafrost thaw on Arctic aquatic ecosystems. *Biogeosciences* **2015**, *12* (23), 7129−7167.
(74) Wu, Y.; Fang, H.; Huang, L.; Cui, Z. Particulate organic carbon dynamics with sediment transport in the upper Yangtze River. *Water Res.* **2020**, *184*, No. 116193.
(75) Yan, Y.; Lauerwald, R.; Wang, X.; Regnier, P.; Ciais, P.; Ran, L.; Gao, Y.; Huang, L.; Zhang, Y.; Duan, Z.; Papa, F.; Yu, B.; Piao, S. Increasing riverine export of dissolved organic carbon from China. *Global Change Biol.* **2023**, *29* (17), 5014−5032.
(76) Soulet, G.; Hilton, R. G.; Garnett, M. H.; Roylands, T.; Klotz, S.; Croissant, T.; Dellinger, M.; Le Bouteiller, C. Temperature control on CO2 emissions from the weathering of sedimentary rocks. *Nat. Geosci.* **2021**, *14* (9), 665−671.
(77) West, A.; Galy, A.; Bickle, M. Tectonic and climatic controls on silicate weathering. *Earth Planet. Sci. Lett.* **2005**, *235* (1−2), 211−228.
(78) Gaillardet, J.; Calmels, D.; Romero-Mujalli, G.; Zakharova, E.; Hartmann, J. Global climate control on carbonate weathering intensity. *Chem. Geol.* **2019**, *527*, No. 118762.
(79) Li, Y.; Li, D.; Liu, G.; Harbor, J.; Caffee, M.; Stroeven, A. P. Patterns of landscape evolution on the central and northern Tibetan Plateau investigated using in-situ produced ^{10}Be concentrations from river sediments. *Earth Planet. Sci. Lett.* **2014**, *398*, 77−89.
(80) Xu, S.; Bufe, A.; Li, S.-L.; Erlanger, E. D.; Ran, L.; Zhong, J.; Yang, C.-J.; Zhang, L.; Ma, T.; Sachse, D. Erosional modulation of the balance between alkalinity and acid generation from rock weathering. *Geochim. Cosmochim. Acta* **2024**, *368*, 126−146.
(81) Mu, C.; Zhang, T.; Zhao, Q.; Su, H.; Wang, S.; Cao, B.; Peng, X.; Wu, Q.; Wu, X. Permafrost affects carbon exchange and its response to experimental warming on the northern Qinghai-Tibetan Plateau. *Agric. For. Meteorol.* **2017**, *247*, 252−259.
(82) Torres, M. A.; West, A. J.; Clark, K. E.; Paris, G.; Bouchez, J.; Ponton, C.; Feakins, S. J.; Galy, V.; Adkins, J. F. The acid and alkalinity budgets of weathering in the Andes−Amazon system: Insights into the erosional control of global biogeochemical cycles. *Earth Planet. Sci. Lett.* **2016**, *450*, 381−391.
(83) Xu, S.; Li, S.; Su, J.; Yue, F.; Zhong, J.; Chen, S. Oxidation of pyrite and reducing nitrogen fertilizer enhanced the carbon cycle by driving terrestrial chemical weathering. *Sci. Total Environ.* **2021**, *768*, No. 144343.
(84) Bufe, A.; Rugenstein, J. K. C.; Hovius, N. CO_2 drawdown from weathering is maximized at moderate erosion rates. *Science* **2024**, *383* (6687), 1075−1080.
(85) Berner, R. A.; Lasaga, A. C.; Garrels, R. M. The carbonate-silicate geochemical cycle and its effect on atmospheric carbon dioxide over the past 100 million years. *Am. J. Sci.* **1983**, *283* (7), 641−683.
(86) Li, L.; Knapp, J. L. A.; Lintern, A.; Ng, G. H. C.; Perdrial, J.; Sullivan, P. L.; Zhi, W. River water quality shaped by land−river connectivity in a changing climate. *Nat. Clim. Change* **2024**, *14*, 225−237.

https://doi.org/10.1021/acs.est.3c06777
Environ. Sci. Technol. 2024, 58, 7032−7044